Comptes Rendus

Mécanique

Michel Visonneau, Ganbo Deng, Emmanuel Guilmineau, Alban Leroyer, Patrick Queutey and Jeroen Wackers

Computational fluid dynamics for naval hydrodynamics

More than a half century of Computational Fluid Dynamics / *Plus d'un demi-siècle de mécanique des fluides numérique*

Computational fluid dynamics for naval hydrodynamics

Michel Visonneau [*, a]**, Ganbo Deng** [a]**, Emmanuel Guilmineau** [a]**,
Alban Leroyer** [a]**, Patrick Queutey** [a] **and Jeroen Wackers** [a]

[a] LHEEA Lab, CNRS UMR 6598, Centrale Nantes, 1 rue de la Noë, B.P. 92101, 44321 Nantes cedex 3, France

E-mails: Michel.Visonneau@ec-nantes.fr (M. Visonneau), Ganbo.Deng@ec-nantes.fr
(G. Deng), Emmanuel.Guilmineau@ec-nantes.fr (E. Guilmineau),
Alban.Leroyer@ec-nantes.fr (A. Leroyer), Patrick.Queutey@ec-nantes.fr (P. Queutey),
Jeroen.Wackers@ec-nantes.fr (J. Wackers)

Abstract. This article describes key issues which have to be addressed to apply Computational Fluid Dynamics to Naval Hydrodynamics. The specific aspects of Naval Hydrodynamics are discussed and illustrated by recent simulations and comparisons with available experiments. Free-surface flows with or without waves and even violent phenomena such as ventilation or cavitation can be modelled with mixture-fluid surface capturing. Turbulence modelling of thick boundary layers and vortical flows requires anisotropic RANS models or hybrid RANS/LES in case of strongly separated flows. Moreover, fluid–structure interaction in the form of rigid or flexible body motion and multi-body systems is crucial to represent ship manoeuvring and propulsion. Finally, the paper underlines the central role played by anisotropic adaptive grid refinement in the accurate simulation of marine flows.

Keywords. Naval hydrodynamics, Turbulence, Scale effects, Fluid–structure interaction, Cavitation, Ventilation, Adaptive grid refinement.

Published online: 8 February 2023

1. Introduction

To address the physical flow configurations relevant to marine engineering, Computational Fluid Dynamics (CFD) has to cope with very diverse and complex flow physics involving (i) free-surface flows with or without incoming waves, (ii) very high Reynolds number ($\approx 10^9$) turbulent flows over complex ship hulls, (iii) interaction between the longitudinal vortical structures developing along the hull in a thick turbulent boundary layer and the rotating propeller or moving appendages located in a highly three-dimensional viscous wake. Moreover, (iv) since the body of interest is free to move at the free-surface with or without incoming waves, the coupling between the flow and the solid motion of the body has to be accounted for. Finally, as the speed is increased, more complex phenomena like ventilation and cavitation might occur and interact, which affects significantly the physics of the flow which has to be simulated.

---

* Corresponding author.

Before the emergence of large computational resources, these phenomena were simulated with a collection of independent and highly specialized tools, mostly inviscid, which were designed to address each peculiar flow situation, such as pure resistance, sea-keeping, propeller flows, etc. From the late eighties, a community of researchers mainly from Europe, the United States, Japan and South Korea had the ambition to build a unique simulation methodology to simulate all these complex phenomena described above. This holistic framework can be summarized as solving the Navier–Stokes equations complemented with *ad-hoc* physical models, like for instance turbulence, cavitation, and laminar-to-turbulence transition models.

The collaborative spirit of these developments is linked with the series of Gothenburg and Tokyo workshops [1,2] which started in 1981 and which were instrumental in defining simulation for naval hydrodynamics as we know it today. Without attempting to be exhaustive, we show a few examples of individual and collaborative work by contributors to these workshops. Advances have been reported in numerical methods (e.g. [3–5]) and the holistic approach has been proven to be valid: the same simulation approach is successful for such diverse subjects as ship wave making [6], manoeuvring [7–11], added resistance in waves [12–14], and propeller analysis [15, 16]. The combination with other models in a multi-physics context has allowed to predict for example cavitation [17,18] and hydrodynamic noise [17,18].

Turbulence, wake flows, and trailing vortices have been a major subject of study over the years. Recent work on turbulence modelling for ship wakes is for example [19–21], while submarines are studied by [22]. Attention has gradually shifted to hybrid turbulence models, which resolve some of the largest turbulent structures and provide higher accuracy for separated flows [23–25]. Also, with the increasing importance of full-scale ship simulation, wall roughness is modelled more and more [26,27].

Finally, the development of CFD methods is not possible without validating the results. The high-quality experimental measurements provided to the community by institutes like IIHR [28,29], NMRI and TUHH [30–32] have been essential for ensuring the standard of numerical simulations today.

In each laboratory or research center, conducting such an ambitious research project needed a team made of researchers putting aside their ego to share the same long-term vision and contribute to the daily development and validation of a common large computational research tool. Such a computational resource, built over the years, is a very valuable asset which can be viewed as the computational counterpart of the large experimental facilities with the same structuring and synergy impact on the research activities.

The CFD methodology was initially based on finite volume or finite difference discretisation on structured grids. Progressively, it became obvious that fully unstructured face-based finite volume discretisation algorithms had to be invented, to account for the complexity of the geometries of interest. Furthermore, such discretisations allow automatic grid adaptation to improve the local and global accuracy of complex flow simulations and significantly reduce the cost of CFD which is more and more expensive, despite the growth of the computational power.

This article shows the authors' vision on how the particular requirements of marine hydrodynamics have shaped the modern CFD solvers dedicated to this domain. Key arguments and illustrations of representative hydrodynamic computations performed with our in-house CFD solver ISIS-CFD will be shown. Whenever possible, comparisons with experiments conducted during the numerous international joint research projects in which the authors were involved during the last thirty years, will be provided. The specific subjects discussed are the simulation of the free surface (Section 2), turbulence modelling and vortical wakes (Section 3), mesh generation with adaptive grid refinement (Section 4) and moving-body dynamics (Section 5). The conclusion summarises these points and discusses the potential for further growth in the following years.

2. Simulating multi-phase flows for marine engineering

2.1. *Numerical framework*

The main particularity of a flow solver for marine applications is the need to consider the free surface. If the water and the air above it are considered immiscible, the water surface appears as a clearly defined interface separating both fluids. Besides a flow discretization, a pertinent numerical method must involve a model for this interface. On the basis of the pioneering work [33], we developed in 2007 [34] a modern free-surface capturing strategy in the context of a unique incompressible fluid model with variable physical properties (density and viscosity). The capturing method allows arbitrary deformations of the air/water interface by solving a water volume fraction equation to determine the amount of each fluid in the cells of the mesh.

The accuracy of such a strategy rests entirely on the capacity of discretisation schemes to capture and convect the contact discontinuity present in the volume fraction. This led to the introduction of so-called compressive schemes which are based on a controlled use of anti-diffusion which aims at maintaining as much as possible the initial discontinuity of the volume fraction. Actually, the first versions of compressive schemes controlling the degree of anti-diffusion needed to prevent and reduce the smearing had limitations in terms of Courant number and density discontinuity. Still based on the Normalized Variable Diagram (NVD) analysis of Leonard [35], robustness and stability for the high density ratio 1:800 for air/water, and up to 1:40,000 for water vapour/liquid water, have been considerably improved in 2011 [36]. In this work, the local monotonicity, the Convection Boundedness Criterion (CBC) rules [37] and the conditions for transparent parallelization for HPC were reinforced.

2.2. *Free-surface examples in calm water*

Integrating a robust free-surface capturing approach in a Navier–Stokes solver opens the way to studying the interaction between the free-surface deformation and the viscous flow field. Traditionally in ship hydrodynamics, it is considered that the free-surface is not influenced by viscosity, which is a justification of model-scale experiments in towing tanks. These experiments are conducted at the same Froude number but at a Reynolds number two to three orders of magnitude lower. Actually, the situation is more complex as revealed by Figure 1 which shows the free-surface elevation, divided by the length between the perpendiculars, L_{PP}, in the wake of a ship at model and full scales. It is clear that the amplitude of the wave created at the stern of the ship depends on the Reynolds number, indicating local and significant scale effects on the free-surface elevation. This phenomenon can be used for example to modify the positioning of a large area propeller (LAP) optimized in full scale conditions and, consequently, increase the propulsive efficiency without suffering from ventilation, as proposed by Knuttson and Larsson [38].

A violent and dangerous free-surface phenomenon is ventilation: the aspiration of air below the surface on a ship propeller, a rudder, or any other lifting surface. Simulating all the phenomena in a ventilating flow is impossible without an accurate and robust representation of the free surface. Figure 2 taken from [39] compares a simulation of a surface-piercing hydrofoil with experiments from Harwood *et al.* [40]. The water-surface model captures the air sheet on the foil surface, the ventilated tip vortex below the foil, the closing of the air pocket behind the foil, and other flow features. The danger of ventilation is that it can appear suddenly, leading to an instant loss of lifting force; Figure 3 shows that even the sudden transition to ventilation can be simulated.
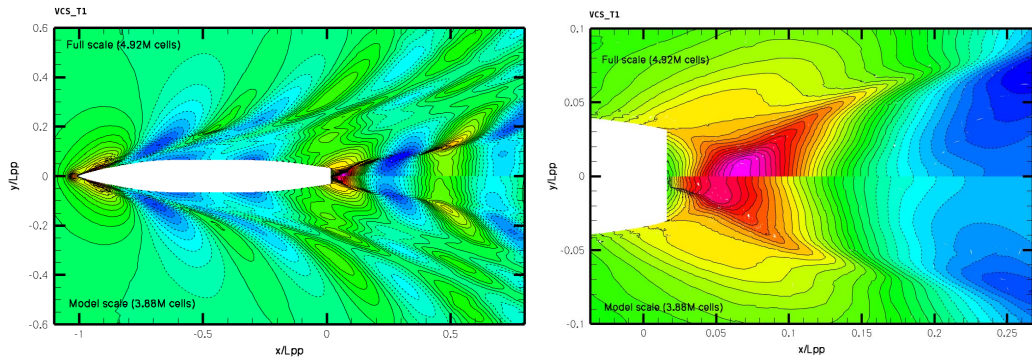
Figure 1. Virtue Container Ship—influence of scale effects on the free-surface elevation. The top half of the figures shows full scale ($Re = 2.89 \times 10^9$), the bottom half model scale ($Re = 1.84 \times 10^7$).
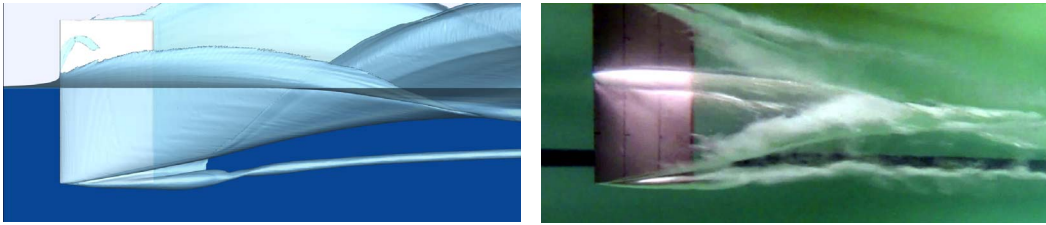

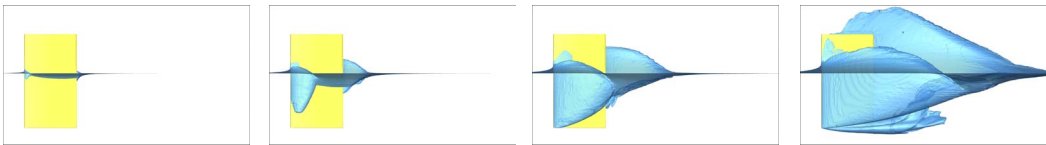**Figure 2.** Ventilating surface-piercing hydrofoil at $\alpha = 15°$: visual comparison with experiments from [40].

Figure 3. Transition to ventilation starting at the upper leading edge for $\alpha = 21.5°$: four snapshots.

2.3. *Wave generation considerations*

The usual, widely documented method for wave generation in CFD is to impose the kinematics of a theoretical potential wave on the boundaries of the computational domain (WBC). However, this approach leaves the challenge of avoiding reflections from the boundaries, especially for long time simulations involving cambered waves. Our alternative solution to this limitation was to introduce an internal wave generator (IWG) as originally proposed by [41]. This method relies on the addition of source terms into the momentum equations to force the velocity components to the desired solution in the domain of interest [42]. It can then be used both to generate waves and to dampen perturbations or reflections.

Based on the work of Fenton [43, 44], a Fourier Series Decomposition method (FSD) of the stream function for irrotational and incompressible is used to generate waves of arbitrary complexity. Moreover, the efficiency of the wave damping has been improved by optimising [45, 46] the strength of the forcing function acting on the source terms of the momentum equations. An example is shown, representative of steep waves in full scale conditions, with a height of 7 m,
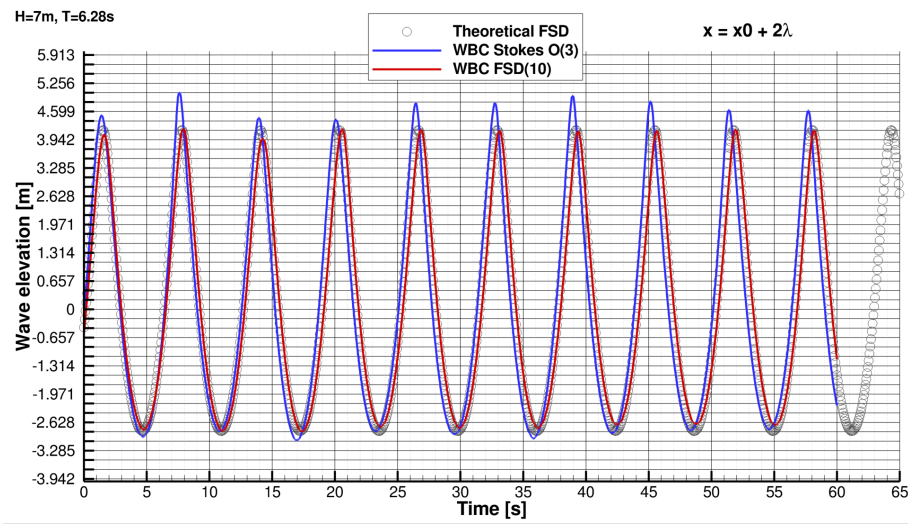
Figure 4. Full scale steep wave generation from boundary. Comparison of the wave elevation 2× past the inlet generator between Stokes Order 3 and a 10 terms Fourier decomposition. Horizontal lines represent the vertical grid resolution.

period 6.28 s and an estimated wavelength of 68.03 m. The time history of the computed wave elevation two wavelengths past the generator inlet is plotted in Figure 4. At the inlet, it is obtained either by the classical Stokes order 3 theory or by a 10 terms decomposition in the FSD series, both with the same damping size and settings. The target wave is perfectly reproduced with the FSD approach whereas instabilities develop with the classical Stokes model.

Another issue is the interaction between the waves and the turbulence model. An example is shown of a wave with period 13.18 s, height 20 m and estimated wavelength λ about 215 m. With such a highly cambered wave, the usual turbulence models will generate too much turbulence production in the fluid, even though the wave kinematics are irrotational. Specific turbulence production limitation at the surface is required, as shown in Figure 5: otherwise, the wave is rapidly dampened and simulation would therefore be valid only over a few waves at this location.

2.4. *Cavitation*

Cavitation is another physical phenomena occurring when dealing with high speed configurations. It also involves two-phase flows but with a higher density ratio ($\approx$40,000) between the two phases of water. It can be modeled using an approach similar to the free-surface but including source terms to reproduce the evaporation/condensation process [17, 18]. The expression of these source terms are defined empirically [47, 48] or based on physical background through a simplified version of the Rayleigh–Plesset equation [49]. This leads to a wide variety of models, but leading to similar results when calibrated on a given case [50]. Figure 6 is an example of a validation which is carried out in collaboration with IRENav of rigid and flexible hydrofoils subject to cavitating flows. The Sauer–Schnerr cavitation model [49] is used. Based on a physical background, this model only depends on the nuclei density n_0 which has physical meaning. It is known that this parameter plays a significant role on the cavitation inception and on the cavitation pattern [51]. Regarding the turbulence model, the k-ω SST model is used with an empirical correction of the eddy viscosity proposed by [52] to counter-balance too much turbulence created at the end of the cavitation pocket. The agreement between measured and computed lift
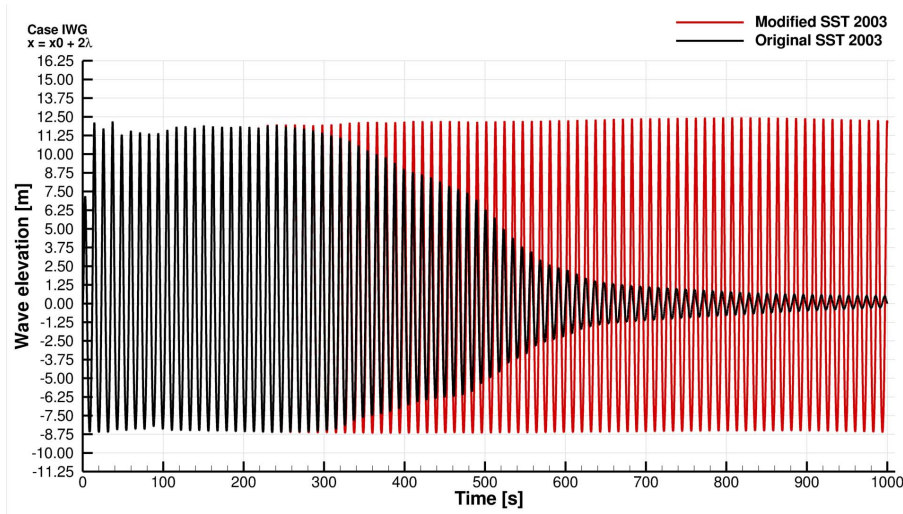
Figure 5. Wave elevation history 2 wavelengths behind the IWG with FSD (10 terms) of the 20 m height wave: effect of the turbulence modelling. Horizontal lines represent the vertical grid resolution.
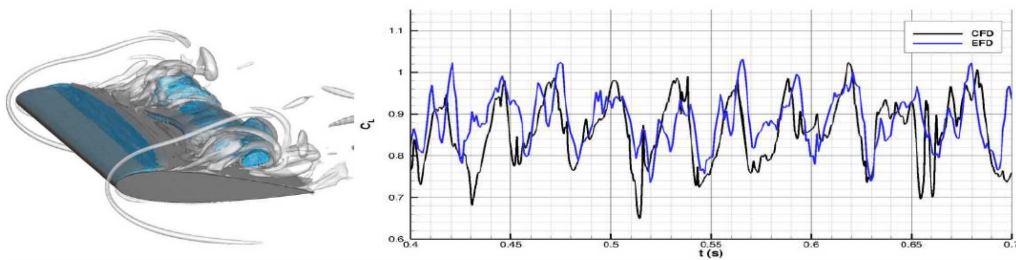

Figure 6. On the left: cavitation patterns (in blue) and main turbulent structures (grey) obtained by simulation. On the right: exp./sim. unsteady comparison of the hydrofoil lift.

is satisfactory despite the well known limitations associated with the linear isotropic turbulence model used in the study.

3. Turbulence modelling

3.1. *Effects of turbulence modelling on the stern flows*

A particular characteristic of ship hydrodynamics is, that a ship is usually an elongated body along which a turbulent boundary layer develops, which gradually thickens. Vital systems for ship propulsion and maneuvering such as the propeller and rudder operate in the wake of the boundary layer at the stern. Moreover, for a U-shaped stern favorable for ship propulsion, bilge vortexes are formed at the stern, which interact with the propeller and the rudder. Hence, the accurate prediction of bilge vortices is crucial in numerical simulation, which is a challenge for statistical turbulence models. It has been found that CFD simulation carried out with linear isotropic eddy-viscosity turbulence models underpredicts the intensity of the bilge vortex. In the early 90's, it was argued that this might be due to numerical discretisation error, neglecting the turbulence modeling errors. However, with the rapid progress of the computer hardware, numerical uncertainty
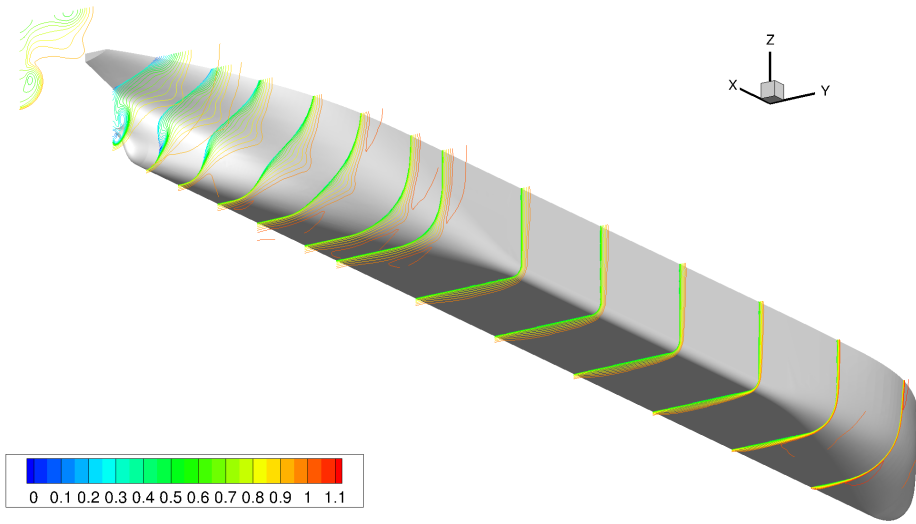
Figure 7. KVLCC2, the geometry and the development of the thickening boundary layer.
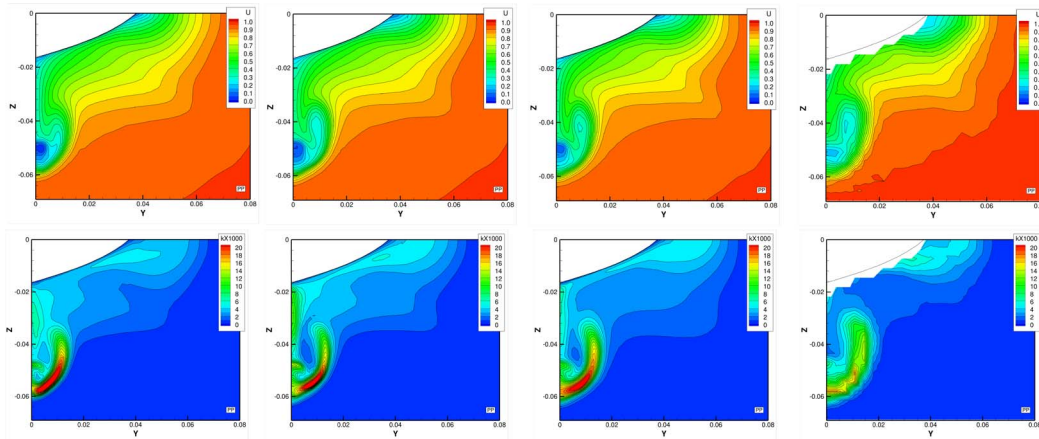

Figure 8. KVLCC2, axial velocity (top) and turbulence kinetic energy (bottom) iso-contours in the propeller plane. Left to right: k-ω SST, EARSM, RSTM SSG/LRR-ω, experiments.

can now be reduced to a small enough level, such that the underestimation of the longitudinal vorticity has been unequivocally attributed to turbulence modeling.

A classic test case is the KVLCC2 [53], a tanker with U-shaped stern lines designed by MOERI, see Figure 7, for which the flow is simulated with Reynolds number $Re = 4.6 \times 10^6$ (neglecting free-surface effects). The iso-wake (streamwise velocity contours) for the KVLCC2 test case at the propeller plane is shown in Figure 8. With a simulation using adaptive grid refinement, the prediction obtained with the k-ω SST model, can be considered a representative grid-independent solution of a linear eddy-viscosity model. The "hook" shape iso-wake observed in the measurements is not correctly captured. This "hook" shape in the velocity contours is the imprint of the bilge vortex formed at the stern.

Inspection of the governing equation for the vorticity reveals that the normal Reynolds stress anisotropy contributes to the formation and the evolution of a vortex. As normal stress anisotropy

cannot be represented with a linear eddy-viscosity model, one way to improve the prediction of a flow containing a vortex is to employ a non-linear turbulence model. Figure 8 shows the prediction obtained by an Explicit Algebraic Reynolds Stress Model (EARSM [54]) specially calibrated by the authors for ship hydrodynamic applications. It is a quadratic non-linear turbulence model based on a two-equation k-ω model. The improvement compared with linear eddy-viscosity can be easily observed. This non-linear turbulence model improves the prediction of the resistance as well. Another alternative to improve the prediction for the bilge vortex is to use a more complex Reynolds Stress Transport Model (RSTM) SSG/LRR-ω [55] for which 7 additional transport equations for the Reynolds stresses and the turbulence frequency of turbulent dissipation are solved. The improvement brought by non-linear turbulence models and Reynolds stress transport models with respect to linear eddy-viscosity models has been confirmed by the results obtained by different organizations using different flow solvers submitted to the Tokyo 2015 CFD workshop [2] devoted to ship hydrodynamics for the JBC test case.

3.2. *Towards hybrid RANS/LES in ship hydrodynamics*

In spite of continuous development for decades since the early 60's, RANS turbulence models still fail to give satisfactory predictions for more complex flows such as flow separation at high rudder angles. Another phenomenon frequently encountered in ship hydrodynamics but poorly modelled with RANS turbulence models is the formation and the evolution of longitudinal vortices along the hull during ship maneuvering. Anisotropic models such as EARSM or RSTM improve the preservation of longitudinal vortices, and the use of wall-resolved boundary conditions rather than wall laws gives somewhat improved prediction of separations. However, none of these models is able to handle strong flow separation or extended vortices accurately.

Large Eddy Simulation (LES) models [25] provide greater accuracy than RANS approaches, but these models suffer from significantly increased computational expenses (mesh size, times) compared to RANS approaches, even in their wall-modelled formulation. As a consequence, the limitations of RANS and the prohibitive cost of LES led to the development of a new class of models, called hybrid RANS/LES models [56]. These models treat the near-wall regions in a manner similar to RANS and the rest of the flow in a manner similar to LES. An excellent review of these hybrid RANS/LES models is provided in a recent publication by Spalart [57]. One of the commonly used models is the DDES (Delayed Detached Eddy Simulation) model [58] which uses the k-ω SST background RANS model and will be used for the next illustration.

The flow around a US-Navy destroyer, the so-called DTMB 5512, see Figure 9, at 10° static drift is investigated with the DDES model and RANS closures [23]. This ship has a length between perpendiculars $L_{PP} = 3.048$ m. The Reynolds number, based on the length L_{PP}, is $Re = 4.65 \times 10^6$ and the Froude number is $Fr = 0.28$.

Figure 10 shows the longitudinal vorticity component and the turbulence kinetic energy in the plane $X/L_{PP} = 0.600$. The onset of the main vortical structures and their trajectories are correctly predicted by all turbulence models although significant differences exist in terms of vortical intensity and detailed vortex core structure. In the same plane, the distribution of turbulence kinetic energy (TKE) is presented in Figure 10. Experiments reveal that a high level of TKE is present in the core of the SDTV vortex, see Figure 9. This high level of TKE is only captured by the hybrid RANS/LES DDES closure which provides results for TKE in very good agreement with the measurements all over the progression of the vortex.

Figure 11 provides a comparison between the measurements and the numerical results for the longitudinal evolution of the cores of the SDTV and BKTV vortices, see Figure 9. The longitudinal velocity component U in the cores of the SDTV and BKTV is reasonably well predicted by all turbulence models. However, the slight increase of U in the SDTV core of the vortex is only
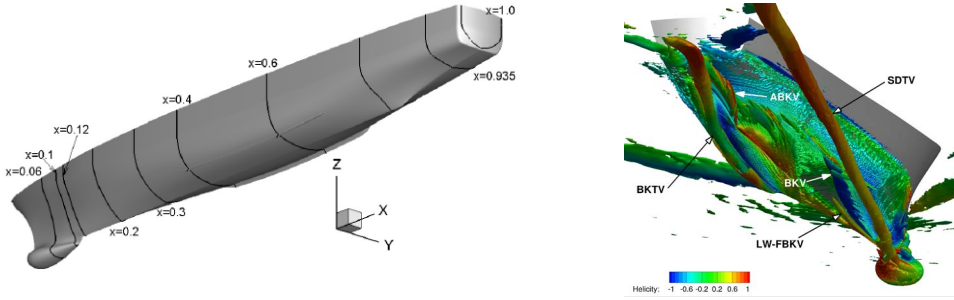
Figure 9. DTMB 5512, the geometry and the experimental measurement locations (left) and vortical structures (right).
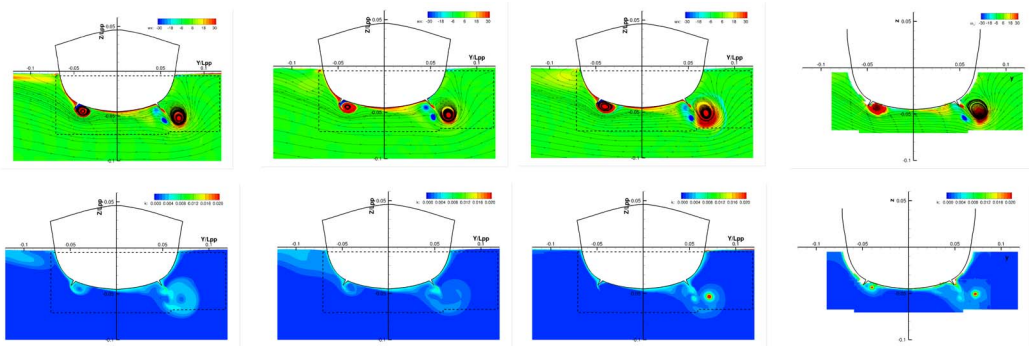

Figure 10. DTMB 5512, longitudinal vorticity component (top) and turbulence kinetic energy (bottom) in the plane $X/L_{PP} = 0.60$. Left to right: k-ω SST, RSTM SSG/LRR-ω, DDES, experiments.

predicted by the DDES model. In the experiments, the TKE in the SDTV core presents a plateau during the progression. This trend is particularly well predicted by DDES, even for the BKTV vortex. k-ω SST and SSG/LRR-ω models underestimate by one to two orders of magnitude the turbulence kinetic energy in the core of SDTV, which shows that the real physics of the flow is not correctly represented by these statistical closures. This high level of TKE is due to the interaction between an inner vortical coherent structure which is meandering and the population of ring vortices surrounding it, see Figure 12. All these unsteady large scale vortices create a high level of velocity fluctuations in the core of SDTV, and, consequently, high level of TKE which is correctly resolved by DDES and cannot currently be predicted by a statistical RANS turbulence model.

4. Adaptive mesh refinement

As seen above, hydrodynamic flows are dominated by localised flow features, such as the free surface but also wakes and trailing vortices. Controlling the numerical error for their simulation requires not only accurate discretisations, but also the ability to capture these features with fine enough grids. However, as the simulation tools evolve and the simulated flows get more and more complex, it is becoming impossible to reliably predict where these fine grids are needed, before the simulation. Thus, either the mesh should be created iteratively, based on the results of preliminary simulations, or large zones must be filled with small cells. Both approaches are so costly in computation and user time that they form a bottleneck for the widespread adoption of complex-flow simulation in hydrodynamics.
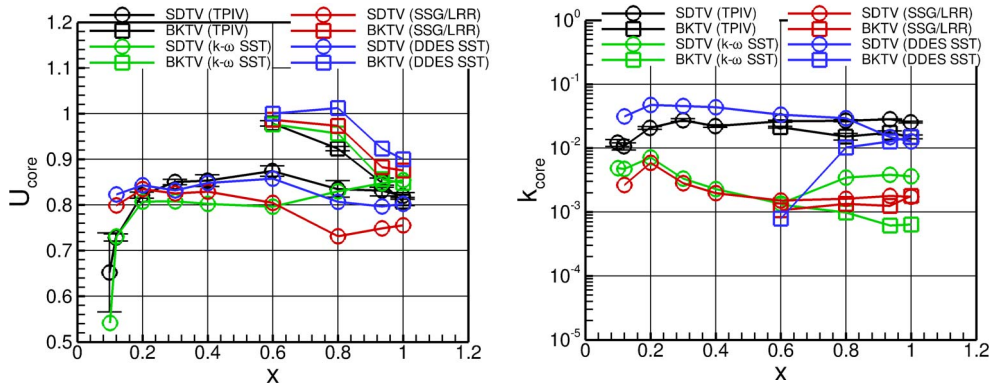
Figure 11. DTMB 5512, longitudinal evolution of the longitudinal velocity component *U* (left) and turbulence kinetic energy *k* (right) along the core of SDTV and BKTV.
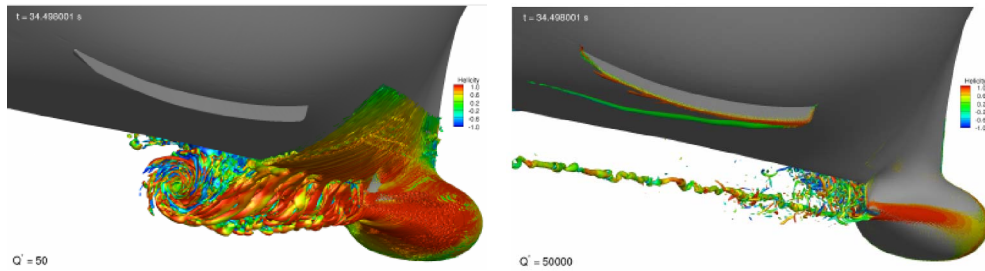

Figure 12. DTMB 5512, view of the iso-Q^* surfaces representing the instantaneous vortical structures that form the SDTV vortex at $X/L_{PP} = 0.30$, (left: $Q^* = 50$), (right: $Q^* = 50,000$).

Adaptive grid refinement, the capacity of a flow solver to dynamically adjust the local mesh size to the requirements of the flow, is a natural solution to this problem. For this reason, mesh adaptation [59] was planned from the beginning for ISIS-CFD. Our original goal was to dynamically mesh the free surface, which besides the compressive discretisation of Section 2.1 requires very fine cells to be captured accurately. Especially in unsteady simulations where the free surface moves during the simulation, the only efficient way to capture the free surface is by inserting the required mesh through adaptive refinement. However, mesh adaptation can do much more and offers the perspective of creating automatically the entire fine mesh needed to capture a complex flow. Today, it is an integral part of our simulation approach: most of the computations presented in this article rely on adaptive mesh refinement.

Technically, complex-flow mesh adaptation is a challenge. We adapt hexahedral meshes by locally dividing the cells into smaller cells. To resolve fine flow features in three dimensions, anisotropic refinement (i.e. the capacity to adjust the aspect ratio as well as the size of the cells adaptively, by dividing cells independently in different directions) is a necessity. Otherwise, features like the free surface or wakes would need to be captured with cubic cells and the sizes of the meshes would be unrealistically high. Compared to isotropic refinement however, where all cells are divided in the same manner, anisotropy adds significant algorithmical challenges. Further difficulties are the need to adapt the mesh in parallel with dynamic load balancing, and the capacity to undo earlier mesh refinement for unsteady flow [59].

The choice where to refine the grid is handled by the refinement criterion, formulated in the metric context [60, 61]. The criterion is a symmetric 3 × 3 tensor field computed from the flow, which indicates the desired local cell sizes in all directions. The actual mesh is then refined to
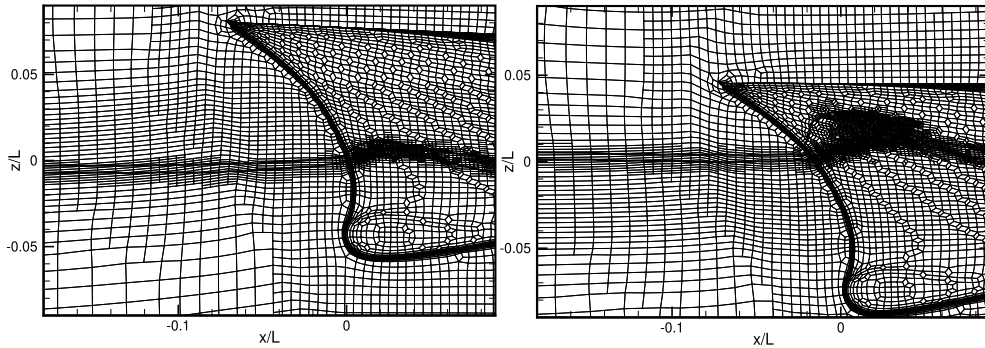
Figure 13. Adapted mesh at the bow of a ship moving freely in waves, shown at the minimum (left) and maximum (right) bow immersion [59].
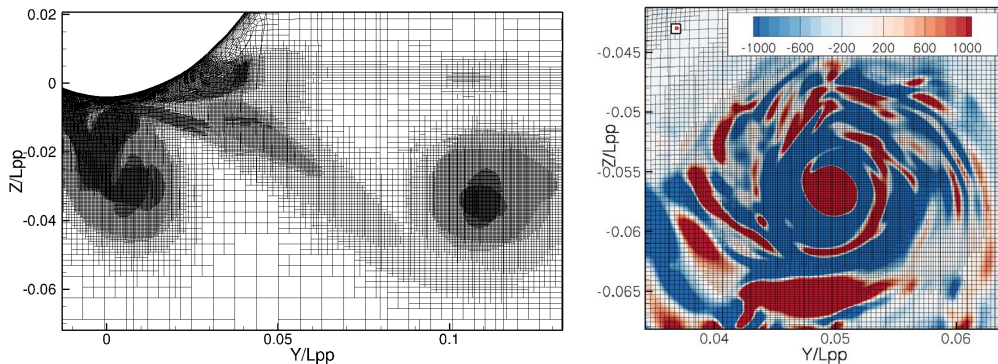

Figure 14. Transversal cut through the adapted mesh for the DTMB 5512 in drift of Section 3 (left) and a detail which compares the adapted mesh in the main vortex core and the resolved flow structures (axial vorticity, right) [62].

fit these sizes as closely as possible. The metric approach is very flexible; we base criteria on the water volume fraction, second derivatives of the flow quantities, and combinations of the two.

Free-surface refinement based on the volume fraction is a standard procedure today. For the ship in waves of Section 5.1 it makes the free-surface capturing easier and more efficient, while it would be impossible to capture all the details of the ventilating flow (Section 2.2) without adaptive refinement. Figure 13 shows another example of mesh adaptation to capture the dynamic motion of a ship in waves. The refined mesh changes as the bow pitches up and down in waves; earlier refinement is completely undone when it is no longer needed.

Figure 14 presents a flow for which all features are captured with adaptive refinement: the trailing vortices behind a ship in drift, simulated with hybrid RANS/LES turbulence modelling as discussed in Section 3. The resolved turbulence is an added challenge for this simulation; in [62] we show that a static mesh based on averaged refinement criteria is the best choice to capture these unsteady flows. For resolved turbulence, mesh refinement is no longer only a means to reduce the numerical error: the mesh resolution and the turbulence model influence each other and have to be mutually adjusted to obtain optimal results.

Thus, mesh adaptation can be used for a large variety of simulation types and it would be impossible to create similar meshes by hand. This shows how adaptive refinement is an essential element for complex-flow simulation.

5. Flow-motion coupling

In marine engineering, the motion of the bodies and the interaction with their environment are of major interest (maneuverability, sea-keeping, etc.). The simple case of the dynamic equilibrium of a hull for a resistance case can be dealt with a quasi-static approach using successive imposed position/orientation increments. However, to solve an unsteady response requires the resolution of the Newton's law coupled with the fluid.

Regarding the structure part, a general parametrisation of the bodies is first required, capable to deal with any 6DOF configuration of possible linked bodies with relative imposed or solved motion (propeller and rudder with hull, etc.) and external forces. A particular attention has to be paid to orientation due to singular configurations (known as Gimbal lock) of any classical parametrisation based on three successive rotations such as Cardan angles. The use of quaternions as internal parameters of orientation nicely tackles this issue, even if the (roll, pitch, yaw) angles remain an easier representation as input and output data.

Compared to aerodynamics where staggered coupling is often used, the co-simulation of the fluid resolution and the structure response in hydrodynamics requires stronger coupling strategies to be robust and stable, due to higher fluid density and a larger added-mass effect. This results in a fluid force greatly dependent on the acceleration of the body. In its turn, this leads to an oscillating diverging behaviour, even for implicit coupling involving a loop of convergence between fluid and structure at the same time step. To reach a stable coupling, a specific treatment of the implicit coupling has to be done by integrating the short term response of the fluid in the structure equation using an approximation of the added-mass operator [63]. This operator can be evaluated and updated during the simulation if needed through the resolution of an elliptic operator inside the Navier–Stokes solver. This specific treatment within the implicit coupling can be also viewed as a physical relaxation [63] or as an iterative resolution of the incomplete LU factorisation of the monolithic fluid–structure system using the computed added-mass operator as an approximation of the Jacobian of the part of the Schur complement involving the inverse of the fluid operator [64]. To be more efficient, it is now common to merge the FSI loop of the implicit coupling with the non-linear loop of the fluid resolution. This results in a so-called internal implicit coupling where the structure resolution is called at each new non-linear iteration using the current fluid forces. The resulting kinematics of the bodies is taken into account by updating the mesh using mesh deformation techniques and/or rigid grid motion to recover body-fitted meshes. Alternatively, boundary conditions can be modified to take into account the modification of the body kinematics within the non-linear iteration through a transpiration method [65] to reduce even more the CPU time. Since several grids can be handled through sliding interfaces and overset domains, single- and multi-body configurations (some of which are presented below) can be carried out, provided that the bodies do not collide.

5.1. *Ship manoeuvrability and seakeeping*

The ability to predict ship motion in calm water and in waves is crucial for the safety of ships and remains one of the challenges of CFD for hydrodynamics. The ultimate goal is to create the numerical tank to avoid tank tests and extrapolation to the real world with at least 3 orders of magnitude on the Reynolds number.

Apart from the above-mentioned six degrees of freedom flow-motion coupling, this requires sliding grids if the propellers are modelled, and overset grids to contain the ship for the interaction with a simulated sea state. From a numerical point of view, the four following conditions must be met: (1) the quality of the generated wave, (2) preventing undesirable effects of reflections during long time simulations, (3) the robustness of the interpolations for inter-domain information transfer to enable self-propulsion and 6DOF resolved free-motion, and (4) intensive
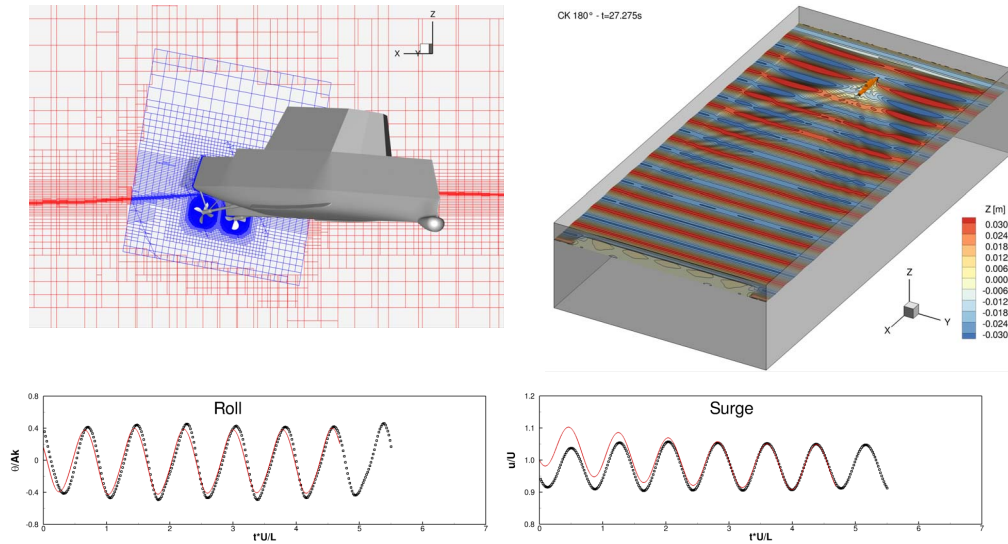
Figure 15. Maneuvering performance of the Office of Naval Research Tumblehome (ONRT) surface combatant model in numerical wave basin. Top left: instantaneous view with two cuts in the adapted grid through the computational domain. Top right: overview of the simulation in following 180° waves when the ship approaches the numerical damping beach. Bottom: comparisons with EFD [66] in usual normalized variables of roll and surge (forward motion), 135° following waves.

use of dynamic adaptive grid refinement to ensure a better capture of the free surface and an optimal mesh continuity in the overlap areas for accurate interpolations.

The representative case illustrated in Figure 15 is drawn from our contributions in various workshops and collaborative NATO-AVT projects in this field. It consists in predicting and comparing the simulated trajectories and motions under the same conditions as the experiments conducted in the IIHR wave basin [66]. The straight path of the model ship with length 3.147 m is maintained by a control law acting on the dynamic positioning of the rudders. In wave (height 0.06294 m and wavelength 3.147 m), the revolution rate of the twin propellers is that computed from self-propulsion in calm water. In these cases of confined domains, the wave field is produced with the help of the internal wave generator as mentioned in Section 2.3.

Additional simulations, this time focused on standardised manoeuvrability exercises, were conducted using the same model and references. These can be found with this animation showing significant vortical structures to be captured in case of zigzag maneuvers https://www.youtube.com/watch?v=5RpZexkz9pY.

While the comparisons in Figure 15 are based on available global data, a detailed understanding of the local interactions requires extensive measurements of the local flow that are still difficult and expensive to deploy. In the absence of such data, and in order to go further in the detailed validation, the following Section 5.2 illustrates the possibilities of CFD for the validation of interactions and efficiency in terms of local forces acting on the propulsion system.

5.2. *Efficiency of electric propulsion in waves*

With the imperative of reducing pollutants and greenhouse gases emissions, electric propulsion for commercial ships, combined with the flexibility of podded propulsors is a promising solution.
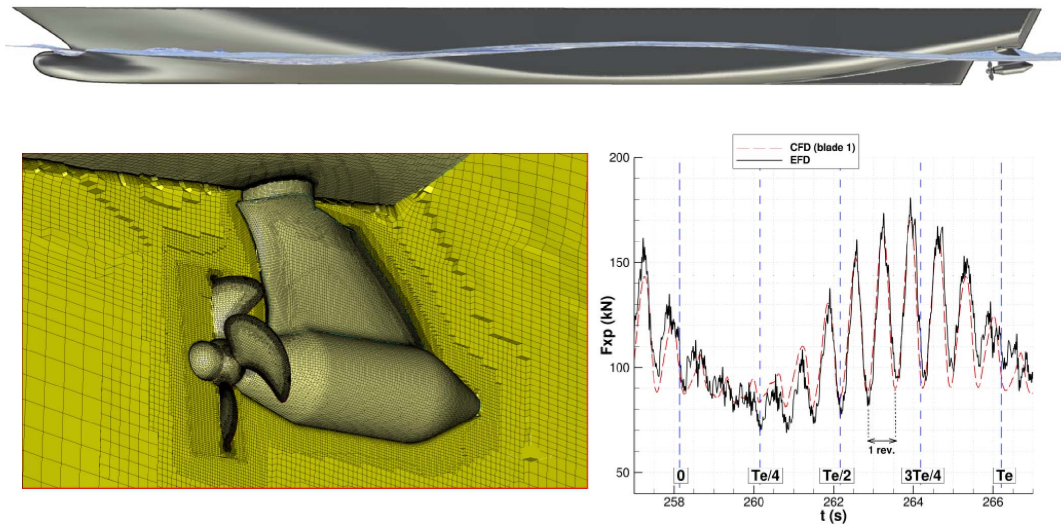
Figure 16. 232 m cruise liner equipped with electric podded system at 11 knots in 4 m wave height. Top: complete model in waves at the time when the maximum loads are predicted. Bottom left: partial view of the grid. Bottom right: single blade thrust in pod reference frame during one encounter wave period (*Te* = 8 s)—CFD in full scale and EFD extrapolated from model scale measurements according to classical rules. See also https://www.youtube.com/watch?v=pe1zac_4GsY.

The STREAMLINE EU-funded FP7 project was the first project for which the effect of waves on cavitation and ventilation was explored in both experimental (EFD) and numerical (ISIS-CFD) ways for a ship with electric pods [67]. The cruise liner ship studied is equipped with a twin-podded system, Figure 16. To measure the propeller efficiency the dynamics of the forces on a single blade and on the complete propeller are measured and compared in blind conditions with the simulations. The level of agreement between CFD and EFD is such that CFD can now be used to perform quantitative analysis of propeller interactions in waves—not only to give a trend.

5.3. *High-fidelity rowing simulator*

Since more than one decade, numerical simulation plays a crucial role in nautical sports, especially in sailing. CFD has become an essential tool for all the design teams of the America's cup for example. In particular, it has greatly helped the rapid development of foiling boats (like AC50 and AC75) with impressive performances. ISIS-CFD plays a peculiar role in this nautical sports environment and has been extensively used by Emirates Team New Zealand during the three last America Cups competitions, leading to two victories in a row during the two last editions of this famous competition.

With the upcoming 2024 Olympic and Paralympic Games in Paris, and the achievements in HPC and in CFD, it was decided to capitalize all the knowledge acquired in a long term research project initiated by the CREPS Pays-de-la-Loire and the French Rowing Federation. The goal of this project is to develop a high-fidelity simulator of the boat-rower(s)-oars system coupled with a CFD flow solver to better understand the physics of this complex mechanical system and thus to support coaches and athletes in the quest of the best performance.
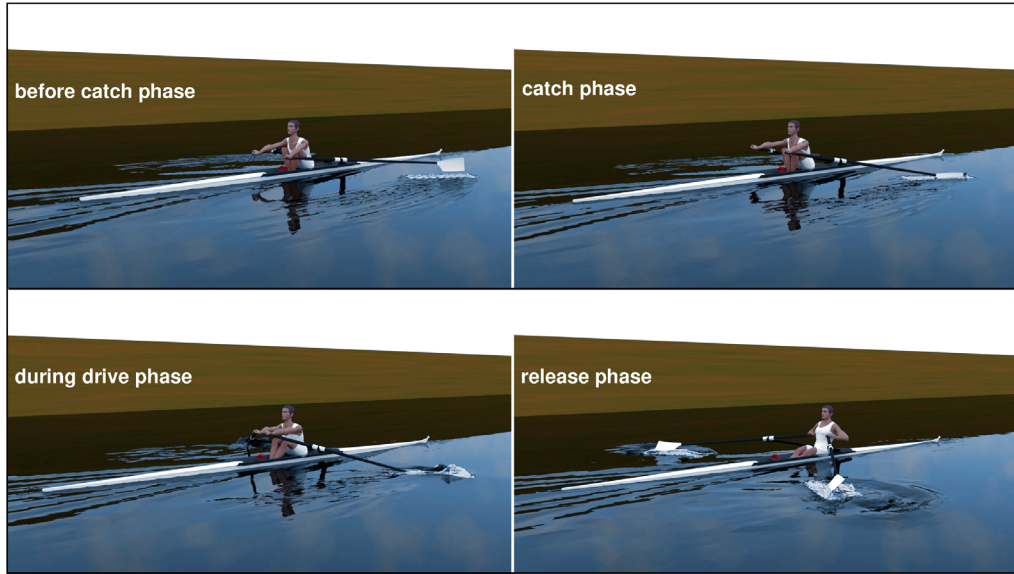
Figure 17. Realistic rendering of the co-simulation SPRing/ISIS-CFD.

Building such a tool is challenging, because the athletes who are the propulsive machine have a strong interaction with the system and use blades which generate a violent unsteady flow. The hull is subjected to large variation of the forward velocity and to large secondary motions (heave and pitch), which are unique features in naval hydrodynamics. From the mechanical system point of view, the equations to solve are similar to the ones used to simulation a self-propelled eel-like body in [68], because both are mechanical systems whose inertia properties change in time. The flexibility of the oar shaft has to be taken into account too [69]. To reach convergence, stabilization techniques based on the evaluation of the added-mass operator are crucial.

To be useful in practice, the so-called SPRing tool (for Simulation of Performance in Rowing) needs accurate models for all the parts (athlete model, kinematics, hydrodynamics, etc.) to be sure that the deduced trends are right. This is all the more crucial since elite athletes already operate near an optimal point. This project also includes the development of realistic rendering of the simulation (see Figure 17) synchronised with specific outputs (hull kinematics, forces, etc.) as a communication facility with coaches, but also as a tool to easier confront the reality with the simulation and analyse the physics.

6. Conclusions and outlook

This article has described key issues which have to be addressed to apply Computational Fluid Dynamics to marine engineering. The need to model and discretise free-surface flows with and without waves is a particular challenge, especially if violent movements like ventilation and cavitation are considered. Surface capturing with a mixture-fluid model is a robust approach to represent all these phenomena. Thick boundary layers and vortical flows, especially longitudinal vortices, are badly resolved by traditional RANS turbulence models. We show that anisotropic turbulence modelling is the key to resolving these flow correctly. Furthermore, flows with strong separations and vortices may reach the limits of RANS modelling; hybrid RANS/LES models provide much better results for these cases, with computational costs that remain lower than LES. Finally, body motion and flow-motion coupling are shown to be essential for representing

among others ship manoeuvring and propulsion. Strong coupling of the fluid and solid solvers, accurate evaluation of added-mass effects, and mesh deformation or multi-domain meshes are important for this. Moreover, the paper underlines the central role played by anisotropic adaptive grid refinement in capturing local flow phenomena like the free surface, wakes, and vortices.

However, although impressive progress has been made regarding numerical accuracy, thanks to the joint development of robust face-based unstructured finite volume discretisations and adaptive grid refinement, we believe that the quest for a higher numerical accuracy (i.e. equal or higher than three) on unstructured grids, should be pursued. This justifies moving from a finite volume framework to a methodology inspired by Discontinuous Galerkin discretisations.

Moreover, the final accuracy of a hydrodynamic simulation depends at the end of the day on the adequacy of the underlying physical models, among which the turbulence model still occupies a central position in 2021, and probably for the next twenty years at least. Contrary to what was planned in the late 90's, a systematic recourse to Wall Modelled Large Eddy Simulation is still impossible for the large Reynolds numbers involved in marine engineering. Despite all the known issues posed by hybrid RANS/LES turbulence models, we believe that these turbulence closures offer the only realistic perspective for improving simulation of turbulent flows over elongated bodies like ships during complex maneuvers. The joint development of Hybrid RANS-LES closures and robust h-p adaptive high order discretisation methodologies will probably shape the future of CFD for marine engineering.

Conflicts of interest

The authors declare no competing financial interest.

Acknowledgments

References

[1] L. Larsson, F. Stern, M. Visonneau (eds.), *Gothenburg 2010, A Workshop on Numerical Ship Hydrodynamics*, Chalmers University of Technology, Gothenburg, Sweden, 2010.

[2] T. Hino, F. Stern, L. Larsson, M. Visonneau, N. Hirata, J. Kim, *Numerical Ship Hydrodynamics, An Assessment of the Tokyo 2015 Workshop*, Springer International Publishing, 2020.

[3] K. Ohashi, T. Hino, H. Kobayashi, N. Onodera, N. Sakamoto, "Development of a structured overset Navier–Stokes solver with a moving grid and full multigrid method", *J. Mar. Sci. Technol.* **24** (2019), no. 3, p. 884-901.

[4] R. Broglia, D. Durante, "Accurate prediction of complex free surface flow around a high speed craft using a single-phase level set method", *Comput. Mech.* **62** (2018), no. 3, p. 421-437.

[5] A. Di Mascio, R. Broglia, R. Muscari, "On the application of the one-phase level set method for naval hydrodynamic flows", *Comput. Fluids* **36** (2007), no. 5, p. 868-886.

[6] H. Raven, "Ship hydrodynamics knowhow derived from computational tools—some examples", in *9th Conference on Computational Methods in Marine Engineering (Marine 2021)*, 2022.

[7] P. Carrica, F. Ismail, H. Hyman, S. Bhushan, F. Stern, "Turn and zig-zag maneuvers of a surface combatant using URANS approach and dynamic overset grids", *J. Mar. Sci. Technol.* **18** (2013), no. 2, p. 166-181.

[8] Y. Sanada, S. Park, D.-H. Kim, Z. Wang, H. Yasukawa, F. Stern, "Experimental and computational study of hull–propeller–rudder interaction for steady turning circles", *Phys. Fluids* **33** (2021), article no. 127117.

[9] S. Toxopeus, C. Simonsen, E. Guilmineau, M. Visonneau, F. Stern, "Viscous-flow calculations for KVLCC2 in maneuvering motion", *J. Mar. Sci. Technol.* **18** (2013), no. 4, p. 460-470.

[10] K. Ohashi, H. Kobayashi, T. Hino, "Numerical simulation of the free-running of a ship using the propeller model and dynamic overset grid method", *Ship Technol. Res.* **65** (2018), no. 3, p. 153-162.

[11] N. Sakamoto, T. Ohmori, K. Ohashi, H. Kobayashi, "False bottoms revisited: computational study for KCS under pure yaw motion in shallow water (H/T = 1.2)", *J. Mar. Sci. Technol.* (2022), p. 1-19.

[12] S. Chen, T. Hino, N. Ma, X. Gu, "RANS investigation of influence of wave steepness on ship motions and added resistance in regular waves", *J. Mar. Sci. Technol.* **23** (2018), no. 4, p. 991-1003.

[13] H. Kobayashi, K. Kume, H. Orihara, T. Ikebuchi, I. Aoki, R. Yoshida, H. Yoshida, T. Ryu, Y. Arai, K. Katagiri, S. Ikeda, S. Yamanaka, H. Akibayashi, S. Mizokami, "Parametric study of added resistance and ship motion in head waves through RANS: calculation guideline", *Appl. Ocean Res.* **110** (2021), article no. 102573.

[14] Y. Sanada, D.-H. Kim, H. Sadat-Hosseini, F. Stern, M. A. Hossain, P.-C. Wu, Y. Toda, J. Otzen, C. Simonsen, M. Abdel-Maksoud, M. Scharf, G. Grigoropoulos, "Assessment of EFD and CFD capability for KRISO container ship added power in head and oblique waves", *Ocean Eng.* **243** (2022), article no. 110224.

[15] J. Andersson, R. Gustafsson, R. Johansson, R. E. Bensow, "Propeller–hull interaction beyond the propulsive factors—a case study on the performance of different propeller designs", *Ocean Eng.* **256** (2022), article no. 111424.

[16] A. Eslamdoost, L. Larsson, R. E. Bensow, "Analysis of the thrust deduction in waterjet propulsion—the Froude number dependence", *Ocean Eng.* **152** (2018), p. 100-112.

[17] R. E. Bensow, G. Bark, "Implicit LES predictions of the cavitating flow on a propeller", *J. Fluids Eng.* **132** (2010), no. 4, article no. 041302.

[18] A. Asnaghi, U. Svennberg, R. E. Bensow, "Large eddy simulations of cavitating tip vortex flows", *Ocean Eng.* **195** (2020), article no. 106703.

[19] T. Hino, K. Suzuki, Y. Takagi, "Modification of k-ω turbulence model for ship resistance flow predictions", *J. Ocean Eng. Mar. Energy* **8** (2022), no. 4, p. 527-538.

[20] T. Xing, S. Bhushan, F. Stern, "DES for a tanker at drift angles with analogy to delta wings", *Ocean Eng.* **55** (2012), p. 23-43.

[21] N. Sakamoto, H. Kobayashi, K. Ohashi, Y. Kawanami, B. Windén, H. Kamiirisa, "An overset RaNS prediction and validation of full scale stern wake for 1600 TEU container ship and 63,000 DWT bulk carrier with an energy saving device", *Appl. Ocean Res.* **105** (2020), article no. 102417.

[22] S. Toxopeus, M. Kerkvliet, R. Vogels, F. Quadvlieg, B. Nienhuis, "Submarine hydrodynamics for off-design conditions", *J. Ocean Eng. Mar. Energy* **8** (2022), no. 4, p. 499-511.

[23] S. Bhushan, H. Yoon, F. Stern, E. Guilmineau, M. Visonneau, S. Toxopeus, C. Simonsen, S. Aram, S.-E. Kim, G. Grigoropoulos, "Assessment of CFD for surface combatant 5415 at straight ahead and static drift $\beta = 20°$", *ASME J. Fluids Eng.* **141** (2019), p. 1-26.

[24] S. Bhushan, H. Yoon, F. Stern, "Detached eddy simulations and tomographic PIV measurements of flows over surface combatant 5415 at straight-ahead and static drift conditions", *Ocean Eng.* **238** (2021), article no. 109658.

[25] N. Alin, R. E. Bensow, C. Fureby, T. Huuva, U. Svennberg, "Current capabilities of DES and LES for submarines at straight course", *J. Ship Res.* **54** (2010), no. 03, p. 184-196.

[26] J. Andersson, D. R. Oliveira, I. Yeginbayeva, M. Leer-Andersen, R. E. Bensow, "Review and comparison of methods to model ship hull roughness", *Appl. Ocean Res.* **99** (2020), article no. 102119.

[27] K. Ohashi, "Numerical study of roughness model effect including low-Reynolds number model and wall function method at actual ship scale", *J. Mar. Sci. Technol.* **26** (2021), no. 1, p. 24-36.

[28] L. Gui, J. Longo, F. Stern, "Towing tank PIV measurement system, data and uncertainty assessment for DTMB model 5512", *Exp. Fluids* **31** (2001), no. 3, p. 336-346.

[29] J. Longo, J. Shao, M. Irvine, F. Stern, "Phase-averaged PIV for the nominal wake of a surface ship in regular head waves", *Int. J. Numer. Meth. Fluids* **53** (2007), no. 2, p. 229-256.

[30] N. Hirata, H. Kobayashi, T. Hino, Y. Toda, M. Abdel-Maksoud, F. Stern, "Experimental data for JBC resistance, sinkage, trim, self-propulsion factors, longitudinal wave cut and detailed flow with and without an energy saving circular duct", in *Numerical Ship Hydrodynamics: An Assessment of the Tokyo 2015 Workshop* (T. Hino, F. Stern, L. Larsson, M. Visonneau, N. Hirata, J. Kim, eds.), Springer, Cham, 2021, p. 23-51.

[31] I. Shevchuk, A. Sahab, M. Abdel-Maksoud, "Experimental and numerical studies of the flow around the JBC hull form at straight ahead condition and 8° drift angle", in *The 33rd Symposium on Naval Hydrodynamics (33rd SNH)*, 2020.

[32] A. Sahab, P. Sumislawski, M. Abdel-Maksoud, "Experimental investigation on the wake of the Japan bulk carrier model with stereoscopic and tomographic particle image velocimetry", in *The 34th Symposium on Naval Hydrodynamics (34th SNH)*, 2022.

[33] O. Ubbink, "Numerical predictions of two fluid systems with sharp interfaces", PhD Thesis, Imperial College of Science, Technology & Medicine, University of London, 1997.

[34] P. Queutey, M. Visonneau, "An interface capturing method for free-surface hydrodynamic flows", *Comput. Fluids* **36** (2007), no. 9, p. 1481-1510.

[35] B. Leonard, "THE ULTIMATE conservative difference scheme applied to unsteady one-dimensional advection", *Comput. Meth. Appl. Mech. Eng.* **88** (1991), no. 1, p. 17-74.

[36] J. Wackers, B. Koren, H. Raven, A. van der Ploeg, A. Starke, G. Deng, P. Queutey, M. Visonneau, T. Hino, K. Ohashi,

"Free-surface viscous flow solution methods for naval hydrodynamic", *Arch. Comput. Meth. Eng.* **18** (2011), no. 1, p. 1-41.

[37] P. H. Gaskell, A. K. C. Lau, "Curvature-compensated convective transport: SMART, a new boundedness-preserving transport algorithm", *Int. J. Numer. Meth. Fluids* **8** (1988), p. 617-641.

[38] D. Knutsson, L. Larsson, "Large area propellers", in *Second International Symposium on Marine Propulsors, smp'11* (Hamburg, Germany), 2011.

[39] M. Charlou, J. Wackers, G. B. Deng, E. Guilmineau, A. Leroyer, P. Queutey, M. Visonneau, "Assessing bi-stable ventilation for surface-piercing hydrofoils through numerical simulation", in *Innov'Sail 2020* (Goteborg, Sweden), 2020 (online).

[40] C. M. Harwood, K. A. Brucker, F. M. Montero, Y. L. Young, S. L. Ceccio, "Experimental and numerical investigation of ventilation inception and washout mechanisms of a surface-piercing hydrofoil", in *30th ONR Symposium on Naval Hydrodynamics* (Hobart, Tasmania), 2014.

[41] J. Choi, S. Yoon, "Numerical simulations using momentum source wave-maker applied to RANS equation model", *Coast. Eng.* **56** (2009), p. 1043-1060.

[42] Z. Li, G. Deng, P. Queutey, B. Bouscasse, G. Ducrozet, L. Gentaz, D. Le Touzé, P. Ferrant, "Comparison of wave modeling methods in CFD solvers for ocean engineering applications", *Ocean Eng.* **188** (2019), article no. 106237.

[43] J. Fenton, "The numerical solution of steady water wave problems", *Comput. Geosci.* **14** (1988), no. 3, p. 357-368.

[44] J. Fenton, "Numerical methods for nonlinear waves", *Coast. Ocean Eng.* **14** (1999), p. 357-368.

[45] R. Perić, M. Abdel-Maksoud, "Analytical prediction of reflection coefficients for wave absorbing layers in flow simulations of regular free-surface waves", *Ocean Eng.* **147** (2018), p. 132-147.

[46] R. Perić, M. Abdel-Maksoud, "Analytical estimate of the reflection coefficient for forcing zones in 3D-flow simulations with nonlinear free-surface waves", in *33rd Symposium on Naval Hydrodynamics* (Osaka, Japan), 2020.

[47] R. Kunz, D. Boger, D. Stinebring, T. Chyczewski, J. Lindau, H. Gibeling, S. Venkateswaran, T. Govindan, "A preconditioned Navier–Stokes method for two-phase flows with application to cavitation prediction", *Comput. Fluids* **29** (2000), no. 8, p. 849-875.

[48] P. Zwart, A. Gerber, T. Belamri, "A two-phase flow model for predicting cavitation dynamics", in *ICMF 2004 International Conference on Multiphase Flow* (Yokohama, Japan), 2004.

[49] J. Sauer, G. Schnerr, "Development of a new cavitation model based on bubble dynamics", *ZAMM—J. Appl. Math. Mech.* **81** (2001), no. S3, p. 561-562.

[50] M. Morgut, E. Nobile, I. Bilus, "Comparison of mass transfer models for the numerical prediction of sheet cavitation around a hydrofoil", *Int. J. Multiphase Flow* **37** (2011), no. 6, p. 620-626.

[51] P. S. Russell, L. Barbaca, J. A. Venning, B. W. Pearce, P. A. Brandner, "The influence of nucleation on cavitation inception in tip-leakage flows", in *34th Symposium on Naval Hydrodynamics*, 2022.

[52] J.-L. Reboud, B. Stutz, O. Coutier, "Two phase flow structure of cavitation: experiment and modeling of unsteady effects", in *3rd International Symposium on Cavitation CAV1998, Grenoble, France*, vol. 26, 1998, p. 1-8.

[53] S. Van, W. Kim, D. Yim, G. Kim, C. J. Lee, J. Eom, "Flow measurement around a 300 K VLCC model", in *Proceedings of the Annual Spring Meeting, SNAK, Ulsan*, 1998, p. 185-188.

[54] G. B. Deng, M. Visonneau, "Comparison of explicit algebraic stress models and second-order turbulence closures for steady flows around ships", in *7th International Conference on Numerical Ship Hydrodynamics*, 1999.

[55] R.-D. Cécora, R. Radespiel, B. Eisfeld, A. Probst, "Differential Reynolds-stress modeling for aeronautics", *AIAA J.* **53** (2015), no. 3, p. 1-17, Published online: 10 September 2014, March 2015.

[56] P. R. Spalart, W. H. Jou, M. Strelets, S. R. Allmaras, "Comments on the feasibility of LES for wings and on a hybrid RANS/LES approach", in *1st AFOSR International Conference on DNS/LES* (C. Z. Liu, ed.), Advances in DNS/LES, Greyden Press, 1997, p. 137-147.

[57] P. R. Spalart, "Chapter four - Hybrid RANS-LES methods", in *Advanced Approaches in Turbulence* (P. Durbin, ed.), Elsevier, 2021, p. 133-159.

[58] M. S. Gritskevich, A. V. Garbaruk, J. Schütze, F. R. Menter, "Development of DDES and IDDES formulations for the k-ω shear stress transport model", *Flow, Turbul. Combust.* **88** (2012), p. 431-449.

[59] J. Wackers, A. Leroyer, G. B. Deng, P. Queutey, M. Visonneau, "Adaptive grid refinement for hydrodynamic flows", *Comput. Fluids* **55** (2012), p. 85-100.

[60] P. L. George, F. Hecht, M. G. Vallet, "Creation of internal points in Voronoi's type method. Control adaptation", *Adv. Eng. Software* **13** (1991), no. 5/6, p. 303-312.

[61] F. Alauzet, A. Loseille, "High-order sonic boom modeling based on adaptive methods", *J. Comput. Phys.* **229** (2010), no. 3, p. 561-593.

[62] S. Mozaffari, E. Guilmineau, M. Visonneau, J. Wackers, "Average-based mesh adaptation for hybrid RANS/LES simulation of complex flows", *Comput. Fluids* **232** (2022), article no. 105202.

[63] C. Yvin, A. Leroyer, M. Visonneau, P. Queutey, "Added mass evaluation with a finite-volume solver for applications in fluid–structure interaction problems solved with co-simulation", *J. Fluids Struct.* **81** (2018), p. 528-546.

[64] M. Durand, A. Leroyer, C. Lothodé, F. Hauville, M. Visonneau, R. Floch, L. Guillaume, "FSI investigation on stability of downwind sails with an automatic dynamic trimming", *Ocean Eng.* **90** (2014), p. 129-139.

[65] S. Deparis, M. A. Fernández, L. Formaggia, "Acceleration of a fixed point algorithm for fluid–structure interaction using transpiration conditions", *ESAIM: Math. Model. Numer. Anal.* **37** (2003), no. 04, p. 601-616, transpiration condition.

[66] Y. Sanada, H. Elshiekh, Y. Toda, F. Stern, "ONR tumblehome course keeping and maneuvering in calm water and waves", *J. Mar. Sci. Technol.* **24** (2019), p. 948-967.

[67] P. Queutey, J. Wackers, A. Leroyer, G. Deng, E. Guilmineau, M. Visonneau, G. Hagesteijn, J. Brouwer, "Dynamic behaviour of the loads of podded propellers in waves: experimental and numerical simulations", in *International Conference on Offshore Mechanics and Arctic Engineering*, vol. 8A: Ocean Engineering, 2014.

[68] A. Leroyer, M. Visonneau, "Numerical methods for RANSE simulations of a self-propelled fish-like body", *J. Fluids Struct.* **20** (2005), no. 7, p. 975-991.

[69] Y. Robert, A. Leroyer, S. Barré, P. Queutey, M. Visonneau, "Validation of CFD simulations of the flow around a full-scale rowing blade with realistic kinematics", *J. Mar. Sci. Technol.* **24** (2018), no. 4, p. 1105-1118.